Growth and Optical Properties of High-Quality Monolayer WS_2 on Graphite

Yu Kobayashi,[†] Shogo Sasaki,[†] Shohei Mori,[†] Hiroki Hibino,[‡] Zheng Liu,[§] Kenji Watanabe,[⊥] Takashi Taniguchi,[⊥] Kazu Suenaga,[§] Yutaka Maniwa,[†] and Yasumitsu Miyata*[,†,∥]

[†]Department of Physics, Tokyo Metropolitan University, Hachioji, Tokyo 192-0397, Japan, [‡]NTT Basic Research Laboratories, NTT Corporation, Atsugi, Kanagawa 243-0198, Japan, [§]Nanotube Research Center, National Institute of Advanced Industrial Science and Technology (AIST), Tsukuba 305-8565, Japan, [⊥]National Institute for Materials Science, 1-1 Namiki, Tsukuba, Ibaraki 305-0044, Japan, and [∥]JST, PRESTO, Kawaguchi, Saitama 332-0012, Japan

ABSTRACT Atomic-layer transition metal dichalcogenides (TMDCs) have attracted appreciable interest due to their tunable band gap, spin-valley physics, and potential device applications. However, the quality of TMDC samples available still poses serious problems, such as inhomogeneous lattice strain, charge doping, and structural defects. Here, we report on the growth of high-quality, monolayer WS_2 onto exfoliated graphite by high-temperature chemical vapor deposition (CVD). Monolayer-grown WS_2 single crystals present a uniform, single excitonic photoluminescence peak with a Lorentzian profile and a very small full-width at half-maximum of 21 meV at room temperature and 8 meV at 79 K. Furthermore, in these samples, no additional peaks are observed for charged and/or bound excitons, even at low temperature. These optical responses are completely different from the results of previously reported TMDCs obtained by mechanical exfoliation and CVD. Our findings indicate that the combination of high-temperature CVD with a cleaved graphite surface is an ideal condition for the growth of high-quality TMDCs, and such samples will be essential for revealing intrinsic physical properties and for future applications.

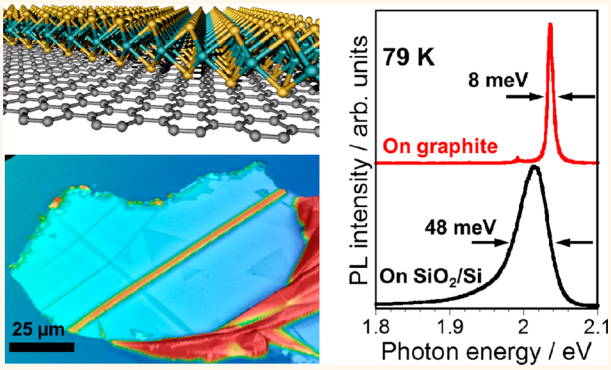

KEYWORDS: WS_2 · graphite · exciton · photoluminescence · line width · CVD growth

Transition metal dichalcogenides (TMDCs) have attracted significant attention in recent years due to their intriguing physical and chemical properties.[1,2] In particular, monolayer Mo- and W-based TMDCs (MoS_2, $MoSe_2$, WS_2, WSe_2, *etc.*), which become direct band gap semiconductors, exhibit excellent on/off current ratios in field-effect transistors (FETs),[3,4] strong photoluminescence (PL),[5−8] and unique spin-valley physics.[9−11] Therefore, TMDCs are expected to be a possible component in future electronic and optoelectronic devices.[1,12] However, the quality of available samples still poses serious problems, such as inhomogeneous lattice strain, charge doping, and structural defects. For example, high-resolution electron microscopy reveals various structural defects, such as monosulfur and disulfur vacancies in TMDCs.[13] PL spectra of as-exfoliated and chemical vapor deposition (CVD) samples often have an asymmetric peak profile and multiple peaks that are probably caused by the presence of charged excitons (trions),[14−17] defect-derived bound excitons,[16,18] and/or neutral free excitons. Such charged and bound excitons also indicate the presence of charged impurities and structural defects. PL peak broadening can also be caused by nonuniform lattice strain.[19] Therefore, there is a strong requirement to develop a method for the preparation of high-quality TMDC samples.

In recent years, many studies have been reported for the growth of high-quality TMDCs, mainly using CVD and metal−film sulfurization.[20−29] In particular, several groups have used atomically flat surfaces of graphite (or graphene) and hexagonal boron nitride (hBN) as the growth substrates of TMDCs.[25−30] Monolayer WS_2 grown by CVD on hBN was very recently reported to exhibit a PL peak with a

* Address correspondence to ymiyata@tmu.ac.jp.

Received for review January 7, 2015 and accepted March 25, 2015.

Published online March 25, 2015
10.1021/acsnano.5b00103

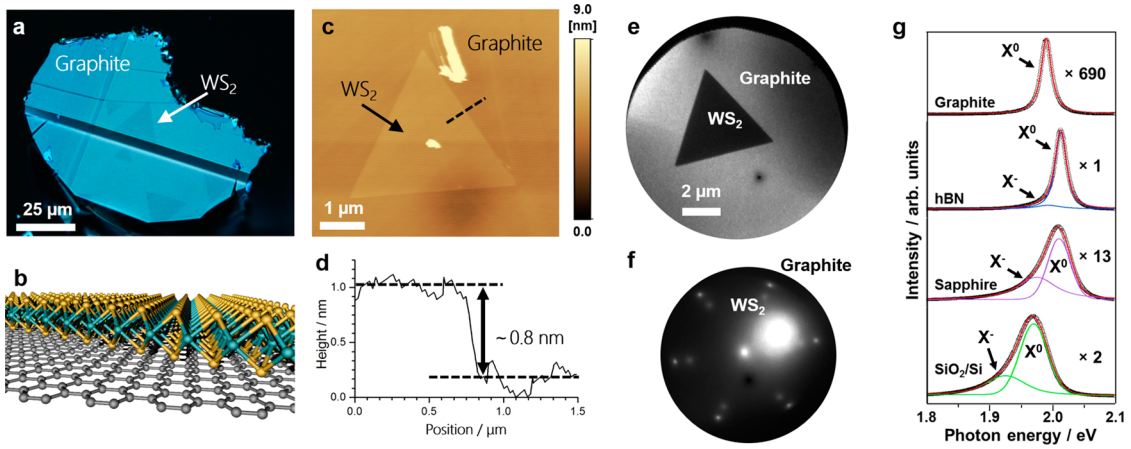

Figure 1. (a) Optical image, (b) structural model, and (c) AFM image of monolayer WS_2 grown on graphite. (d) Height profile of the dotted line in (c). (e) LEEM image and (f) LEED pattern of monolayer WS_2 grown on graphite. The electron beam energies were 11 and 45 eV for LEEM and LEED observations, respectively. (g) Room-temperature PL spectra of monolayer WS_2 grown on graphite, hBN, sapphire, and SiO_2/Si substrates. There are two peaks, which are the neutral exciton (X^0) and the lower energy charged exciton (X^-).

relatively narrow full-width at half-maximum (fwhm) of 26 meV and a weak asymmetric profile.[25] Considering monolayer growth on commonly used substrates such as SiO_2/Si and sapphire, this indicates that the growth substrate is one of the essential factors for reducing charged impurities and structural defects. Even though such effort has been devoted for improving the growth conditions, the optical spectra of CVD samples are still much different from the high-quality $MoSe_2$ monolayers obtained by mechanical exfoliation.[16] This high-quality $MoSe_2$ shows two PL peaks of neutral and charged excitons with a symmetric profile and a very narrow fwhm of 5 meV at 15 K for neutral exciton. These situations indicate that the CVD growth of high-quality TMDC samples without carrier doping is still a challenging issue.

Here, we report the growth of high-quality monolayer WS_2 on a cleaved graphite surface by CVD under exceptionally high-temperature conditions at 1100 °C. The single-crystal domains are triangular shaped with sizes of up to 15 μm. PL and Raman spectroscopy reveal the uniformity and quality of WS_2 samples grown on graphite, hBN, SiO_2/Si, and sapphire substrates. The PL spectra of WS_2 samples grown on graphite have almost perfectly symmetric Lorentzian profiles and a narrow fwhm of 21 meV at room temperature and 8 meV at 79 K. Furthermore, there are no additional peaks due to charged and/or bound excitons, even at low temperature, which suggests that there are very few charged impurities and structural defects. These results indicate that the combination of high-temperature CVD with a cleaved graphite surface provides an ideal way to grow high-quality, nondoped TMDCs.

RESULTS AND DISCUSSION

Figure 1a presents an optical image of triangular-shaped WS_2 grains that have relatively dark contrast on graphite. That structure model is shown in Figure 1b. Atomic force microscope (AFM) observation reveals that a similar WS_2 grain has a uniform height of around 0.8 nm (Figure 1c,d), which indicates these grains correspond to monolayer WS_2. Figure 1e shows a low-energy electron microscopy (LEEM) image of monolayer WS_2 on graphite. The low-energy electron diffraction (LEED) pattern of this area shows two hexagonal patterns, which are derived from graphite for the outer spots and from the monolayer WS_2 for the inner spots (Figure 1f). This hexagonal pattern of the WS_2 means that such triangular-shape grains are single crystals, which is also confirmed from dark-field LEEM images (Figure S1a,b). Note that the LEED patterns become 3-fold symmetric depending on the electron beam energy, due to the symmetry of its crystal structure (Figure S1c,d,e). These two hexagonal patterns clearly indicate that the monolayer WS_2 crystal has the same crystal orientation as the graphite substrate.

In addition to the monolayer WS_2, multilayer WS_2 grains are frequently observed on the graphite (Figure S1f). At optimized growth conditions, the ratio of monolayer to multilayer grains is roughly around 0.1. For the multilayer grains, LEEM and LEED results strongly suggest that they tend to have a random orientation (Figure S1g,h,i). These differences in the crystal orientation probably result from the nucleation process in the crystal growth. Here, we will focus our attention on the optical properties and quality of monolayer WS_2 grown on graphite and other substrates.

Figure 1g shows representative room-temperature PL spectra for monolayer WS_2 grown on graphite, hBN, sapphire, and SiO_2/Si substrates. Except for the hBN sample, the spectra were measured for triangular-shaped single crystals with sizes around 10 μm, as shown in Figures 2a, 3a, and 4a. Note that the monolayer WS_2 crystals on hBN are mainly less than 1 μm in size with the growth conditions employed,

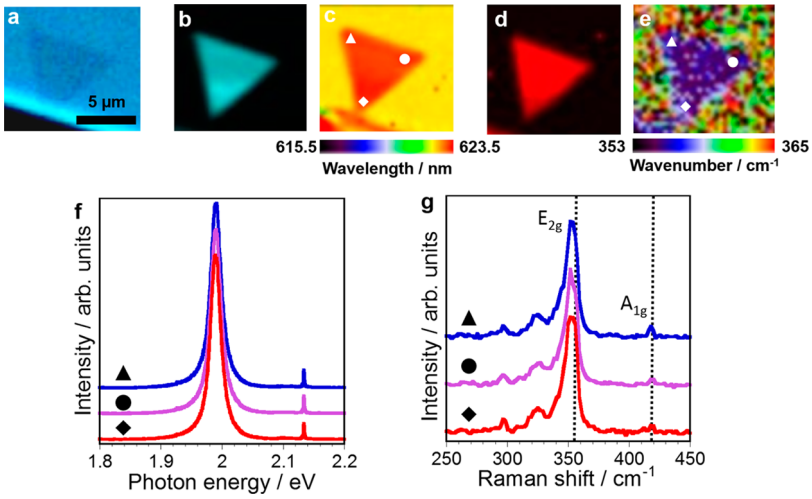

Figure 2. (a) Optical image, (b) PL intensity, and (c) peak wavelength maps and (d) E_{2g} Raman mode intensity and (e) peak wavenumber maps for monolayer WS_2 grown on graphite. (f) PL and (g) Raman spectra measured at three different points indicated by the symbols in (c) and (e), respectively.

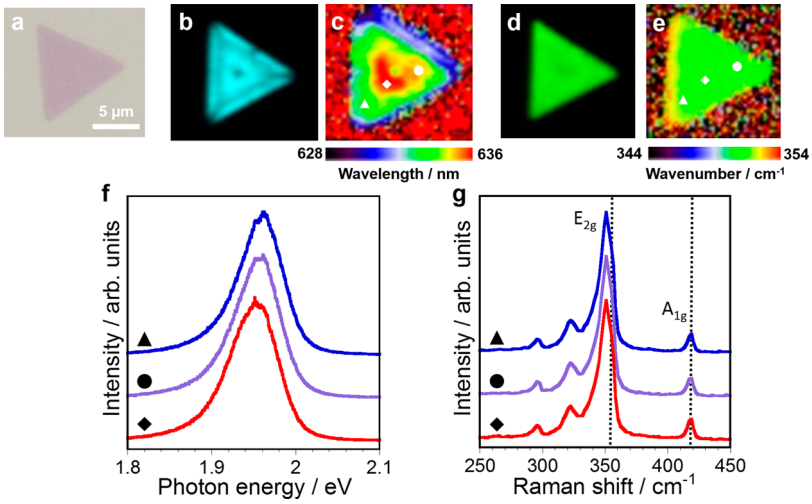

Figure 3. (a) Optical image, (b) PL intensity, and (c) peak wavelength maps and (d) E_{2g} Raman mode intensity and (e) peak wavenumber maps for monolayer WS_2 grown on SiO_2/Si. (f) PL and (g) Raman spectra measured at three different points indicated by the symbols in (c) and (e), respectively.

probably due to the different surface properties of hBN. On the SiO_2/Si substrates, WS_2 crystals were grown by the thin film sulfurization method at relatively low temperature (900 °C) to avoid the reaction of Si with sulfur. These four spectra present PL peaks with different intensity, peak energies, line widths, and profiles, as summarized in Table S1.

The PL peaks for WS_2 on graphite and hBN have similar symmetric profiles and small fwhm's, whereas for WS_2 on sapphire and SiO_2/Si, asymmetric and broad peaks are observed. Only the PL spectrum for WS_2 on graphite is well fitted by a single Lorentzian function, as shown in Figure 1g. For the other substrates, each peak can be reproduced by two Voigt function components. (The peak energies, fwhm, and peak-area ratios are given in Table S2.) For the asymmetric peaks, the components at lower and higher energies are assigned to the emission from trions and neutral free excitons, respectively.[14−17] The presence of both free excitons and trions indicates that there is local charge doping in the as-grown samples.

The fwhm values are 21, 22, 53, and 61 meV for the WS_2 samples on graphite, hBN, sapphire, and SiO_2/Si, respectively. The WS_2 samples on sapphire and SiO_2/Si have comparable fwhm values to those previously reported for CVD-grown and exfoliated monolayer WS_2 on Si substrates.[5,15,30] In contrast, the fwhm values for the WS_2 samples on graphite and hBN are less than half, which suggests fewer defects and charged impurities in the WS_2. This is also supported by high-resolution transmission electron microscope (HRTEM) observations. As shown in Figure S2, a clear lattice image and electron diffraction pattern are observed for few-layer WS_2 grown on monolayer graphene. Even though the peak profiles are similar at room temperature, the spectra for on graphite and hBN measured at

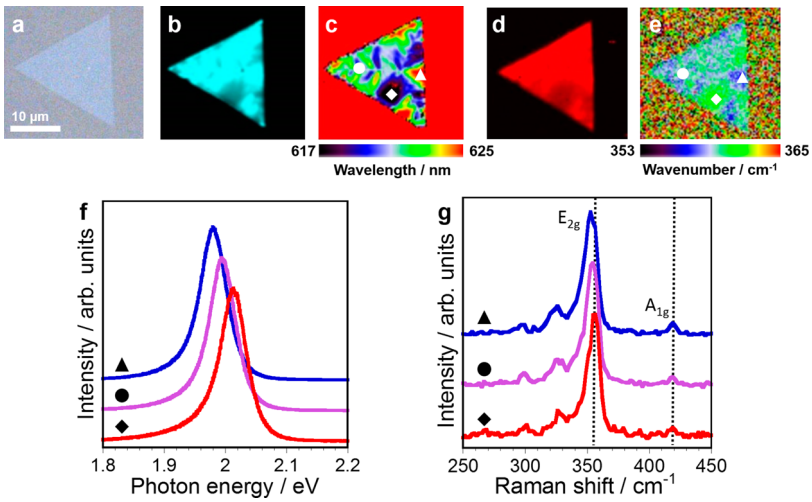

Figure 4. (a) Optical image, (b) PL intensity, and (c) peak wavelength maps and (d) E_{2g} Raman mode intensity and (e) peak wavenumber maps for monolayer WS_2 grown on sapphire. (f) PL and (g) Raman spectra measured at three different points indicated by the symbols in (c) and (e), respectively.

79 K are much different, as discussed later (Figures S7 and S8).

For the PL intensities, the monolayer WS_2 samples on hBN and SiO_2/Si exhibit comparable, intense signals. On sapphire, the PL intensity decreases to around 1/6, which suggests relatively low sample quality of the WS_2 on sapphire. It is noteworthy that the PL intensity of monolayer WS_2 on graphite is 2 orders of magnitude less than that on hBN, although they have almost the same fwhm values. This can be interpreted as the presence of a fast nonradiative recombination process of WS_2 on graphite.

The dependence of the peak energy on the substrate is attributed to the effect of both lattice strain and dielectric screening. Dielectric screening is also known to affect the excitonic transition energy of other low-dimensional semiconductors, such as single-wall carbon nanotubes (SWCNTs).[31] The relative lattice strain is estimated from Raman measurements, as reported previously.[32,33] PL and Raman mapping was conducted to investigate the uniformity within the single crystals in addition to the substrate effect.

Figures 2−4 and S3 show the PL and Raman imaging results for WS_2 on the four substrates. For WS_2 on graphite, the PL and E_{2g} Raman mode peak positions are uniform within the single crystals (Figure 2c,e,f,g). Similar results were also obtained for the peak intensity maps (Figure 2b,d). These results indicate that the lattice strain and electronic properties of WS_2 are uniform on the graphite substrates.

However, WS_2 on the sapphire and SiO_2/Si substrates presents a noticeable variation in PL and/or Raman peaks (intensities), even within a single crystal (Figures 3 and 4). These variations are probably caused by inhomogeneous lattice strain, charged impurities, and structural defects of the samples. In particular, for the WS_2 on a sapphire substrate, there is a strong correlation between the PL peak wavelength (energy) and the E_{2g} mode wavenumber, which indicates that the PL shift is derived from lattice strain, as reported previously.[19] The PL peak energy increases from 1.98 to 2.01 eV (Figure 4f) as the E_{2g} wavenumber increases from 353 to 356 cm^{-1} (Figure 4g). As predicted theoretically,[34] the band gap becomes larger by compressive strain, which can be detected as E_{2g} phonon hardening, and this tendency is consistent with the previous experimental reports.[19,32,33]

Compared with WS_2 on the sapphire substrate, WS_2 on the SiO_2/Si substrates exhibits a lower PL peak energy (1.97 eV) and a lower E_{2g} phonon energy (349 cm^{-1}). This relationship can also be explained by the lattice strain effect, which is attributed to the substrate-dependent thermal expansion coefficient (TEC) and the interaction between monolayer WS_2 and each substrate. The values of TEC are around 6.35, −1.5−0.9, −2.72, 7.5−8.5, and 0.50 μ/K for bulk WS_2, graphite, hBN, sapphire, and SiO_2, respectively.[35−38] The large TEC for the sapphire substrate means that the cooling process after WS_2 growth leads to thermal shrinking, which could introduce compressive strain into WS_2. The small TEC for the SiO_2 substrate could prevent the thermal shrinking of WS_2 during the cooling process, and thereby tensile strain would be introduced into WS_2 at room temperature. Even though graphite and hBN have similar TECs to SiO_2, the E_{2g} wavenumbers on graphite and hBN substrates are intermediate between those on SiO_2/Si and sapphire. This situation suggests that WS_2 monolayers on graphite and hBN have less strain than that on SiO_2/Si and sapphire. This is attributed to the fact that the cleavage surfaces of these substrates would impart very low lateral frictional force because they are atomically flat and ultraclean. Actually, graphite and hBN have a smoother surface than SiO_2/Si and sapphire, as shown in Figure S4. The values of

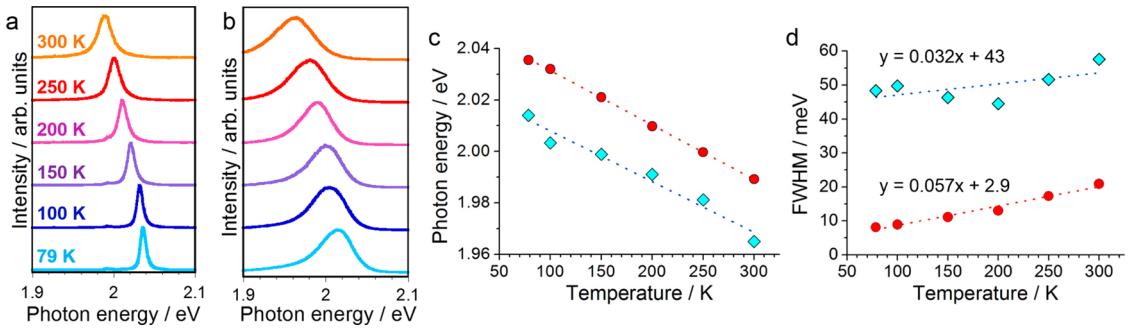

Figure 5. Temperature-dependent PL spectra for monolayer WS_2 on (a) graphite and (b) SiO_2/Si substrates. (c) Peak energies and (d) fwhm plotted as a function of temperature for graphite (red circles) and SiO_2 (blue diamonds). Small peaks around 1.996 eV in (a) are derived from the 2D mode Raman scattering of graphite.

root-mean-square roughness are 87 and 68 pm for graphtie and hBN substrates, respectively, which are approximately half of those of sapphire (161 pm) and SiO_2/Si (158 pm).

It is noteworthy that the WS_2 on sapphire is comparable in emission energy to the WS_2 on hBN. This is probably due to the dielectric screening effect on the exciton binding energy, as observed for SWCNTs.[31] Briefly, the exciton transition energy decreases with an increase in the dielectric constant of the surrounding medium. Sapphire has a larger dielectric constant of 9.4−11.6 than that of hBN (3−4).[39,40] This large dielectric constant of sapphire could lower the emission energy of WS_2. In the case of SiO_2 and hBN, SiO_2 has a similar dielectric constant of 3.9 to hBN. Considering the difference in E_{2g} wavenumbers, the lattice strain could be a major factor for the lower PL peak energy for WS_2 on SiO_2/Si. For graphite and hBN, their E_{2g} wavenumbers are almost the same values, whereas metallic graphite has a stronger screening effect than insulating hBN. This could lower the PL peak energy of WS_2 on graphite. These results strongly suggest that the lattice strain and screening effects from the substrates play important roles in the electrical and optical properties of CVD-grown WS_2 on these substrates.

Temperature-dependent PL spectra were measured to obtain further insight into the line width and the structural defects of WS_2. Figures 5 and S5 present temperature-dependent PL spectra for monolayer WS_2 grown on the graphite and SiO_2/Si substrates. For comparison, the PL peak energies and the fwhm values are plotted in Figure 5c and d. Both samples exhibit an upshift of PL with decreasing temperature, as observed for common semiconductors.[41] It should be noted that for the graphite sample the line width becomes sharper from 21 meV at room temperature to 8 meV at 79 K. This value (8 meV at 79 K) is comparable to that of high-quality, exfoliated $MoSe_2$ monolayers reported previously (5 meV at 15 K).[16] It is worth noting that, unlike the $MoSe_2$, the present WS_2 exhibits only a single peak at 79 K because of the absence of a charged exciton peak, which indicates less charged impurities. In the case of the SiO_2/Si substrate, the line width at 79 K is still large (around 40−50 meV), which is close to that at room temperature (45−60 meV), as shown in Figure S5. This weak temperature dependence of the line width and inhomogeneous broadening of the PL peak is evidence for the microscopic distribution of lattice strain and charged impurities. In contrast, the graphite substrate provides an ideal condition for WS_2 without such inhomogeneous factors due to its atomically flat and impurity-free surface.

Similar results can be obtained for monolayer MoS_2 grown on graphite. As shown in Figure S6, the MoS_2 grown on graphite also has a single, relatively narrow PL peak with symmetric profile and temperature-dependent line width. Furthermore, no additional peaks are observed for charged and/or bound excitons at low temperature. The temperature dependence of the line width also suggests the difference in the degree of exciton−phonon interaction between WS_2 and MoS_2 monolayers. These results show that the present high-temperature growth on graphite provides a useful way for the preparation of high-quality and nondoped TMDCs with various compositions.

Finally, it is noted that multiple peaks often appear at low temperature or under vacuum for the WS_2 on hBN and SiO_2/Si samples (Figures S7 and S8). These peaks can be attributed to trion or defect-derived bound excitons.[16,18] Such multiple peaks were not observed for WS_2 on the graphite substrate even at 79 K, which suggests fewer structural defects and charged impurities in the monolayer WS_2 crystals grown on graphite. One may think that the charge transfer with substrates may be a major factor to modulate PL spectra of WS_2 on graphite. To investigate the influence of substrates, WS_2 monolayers were transferred from a SiO_2/Si substrate as a growth substrate onto exfoliated graphite and another SiO_2/Si substrate. Despite the presence of a strong interlayer interaction as indicated by the PL quenching, the transferred WS_2 on graphite has an asymmetric PL peak with a very large fwhm value of 90 meV (Figure S9). Furthermore, the peak profiles are similar between WS_2 monolayers on graphite and SiO_2/Si. This result also supports that the WS_2 monolayers

directly grown on graphite have an intrinsically high quality.

These optical responses indicate that, under vacuum, WS_2 monolayers on hBN have much more electron concentration in the conduction band than those on the other substrates. This causes the increase of PL intensity of the neutral exciton through the charge transfer with adsorption of gas molecules such as oxygen and water. In contrast, WS_2 monolayers on the other substrates are insensitive to the gas adsorption because the lower electron concentration suppresses the charge transfer. The origin of this substrate dependence could be the effect of substrates and/or impurities. The presence of an additional peak in the hBN sample may be related to the small WS_2 grain sizes of around 1 μm. For such small grains, the edge effect could dominate the optical properties of the TMDCs. Thus, further improvement of the growth conditions would provide high-quality WS_2 on hBN, which is highly desirable for various electronics applications.

CONCLUSION

It is concluded that the combination of high-temperature CVD with a cleaved graphite surface is an ideal condition for TMDC growth with a large grain size and uniform optical properties. In particular, CVD-grown monolayer WS_2 on graphite gives rise to a single PL peak with a symmetric Lorentzian profile and very small fwhm values of 21 meV at room temperature and 8 meV at 79 K. Compared with WS_2 on sapphire and SiO_2/Si substrates, the WS_2 grown on graphite is less affected by charged impurities and structural defects. The present findings should pave the way for the preparation of high-quality and nondoped TMDCs, and such samples will enable further investigation into the intrinsic properties of TMDC atomic layers.

METHODS

Monolayer WS_2 grains were grown on Kish graphite (type C or B, Covalent Materials Co.), hBN, and c-plane sapphire (OS Tech Co., Ltd.) substrates using an improved CVD method[21−23] and on a SiO_2/Si (100 nm SiO_2) substrate by thin-film sulfurization.[24,30] Single-crystal hBN was prepared by a high-temperature and high-pressure method.[42] First, graphite and hBN crystals were mechanically exfoliated onto quartz substrates using Nitto tape (SPV-224). The optical image and Raman spectra of exfoliated graphite and hBN are shown in Figure S10.

For CVD growth, the substrate was placed in a quartz tube (3 cm diameter, 100 cm long) with WO_3 powder (Aldrich, 99% purity, 15−50 mg) and sulfur flakes (Aldrich, 99.99% purity, 2 g). The quartz tube was then filled with Ar gas at a flow rate of 100 cm^3/min. The temperature of the substrate and the WO_3 powder was gradually increased to the sulfurization temperature (900−1100 °C) over 60 min using an electrical furnace. When the substrate temperature was at the set point, the sulfur was heated at 200 °C for 15−30 min to supply sulfur vapor to the substrate using another electrical furnace. After sulfurization, the quartz tube was immediately cooled using an electric fan. For the thin-film sulfurization method, the WO_3 film was deposited onto a SiO_2/Si substrate in a striped shape using a shadow mask. The substrate was placed in the quartz tube with the sulfur flakes as previously described. The quartz tube was filled with Ar gas at a flow rate of 200 cm^3/min. The substrate and the sulfur were heated at 900 and 190 °C, respectively, for 30 min to conduct the sulfurization process. For the SiO_2/Si substrate, sulfurization was conducted at a lower temperature than the other substrates to avoid the reaction of Si and sulfur.

Optical images were recorded with an optical microscope (Nikon, Eclipse-LV100D). Raman measurements were conducted using a micro-Raman spectroscope (Renishaw, inVia) with an excitation laser at 532 nm. The temperature-dependent PL measurements were performed with a temperature-controlled microscope system (Linkam, THMS-350 V) under vacuum at 20 Pa. Topography images of the sample were obtained by using AFM (Shimadzu, SPM-9600) in tapping mode. A LEEM instrument (Elmitec LEEM III) was used to obtain bright-field and dark-field images and LEED patterns of WS_2 on graphite. A field emission JEM-2010F equipped with a spherical aberration (C_s) corrector (CEOS) was operated at 120 kV for the HRTEM imaging with high resolution and high contrast. The specimen was observed at room temperature. The C_s was set to less than 1 μm. A Gatan 894 CCD camera was used for digital recording of the HRTEM images. A sequence of HRTEM images (20 frames) was recorded, with an exposure time of 1 s for each. After drift compensation, some frames can be superimposed to increase the signal-to-noise ratio for display. HRTEM images are filtered by a commercial software named HREM-Filters Pro.

Conflict of Interest: The authors declare no competing financial interest.

Supporting Information Available: Table of PL peak energy, PL fwhm, and E_{2g} Raman mode peaks for monolayer WS_2 grown on graphite, hBN, sapphire, and SiO_2/Si substrates (Table S1). Table of fitting parameters used for Figure 1g (Table S2). Dark-field LEEM images and LEED patterns of monolayer WS_2 on graphite, optical and LEEM images and LEED patterns of multilayer WS_2 on graphite (Figure S1), HRTEM image and electron diffraction pattern of few-layer WS_2 grown on monolayer graphene (Figure S2), Raman spectra for WS_2 grown on graphite, hBN, sapphire, and SiO_2/Si substrates (Figure S3), AFM images of graphite, hBN, sapphire, and SiO_2/Si substrate surfaces (Figure S4), temperature-dependent PL for two different WS_2 crystals on SiO_2/Si substrates (Figure S5), PL spectra of MoS_2 grown on graphite and SiO_2/Si substrates (Figure S6), temperature-dependent PL spectra for monolayer WS_2 grown on hBN and on SiO_2/Si substrates (Figure S7), AFM image, height profile, and temperature-dependent PL spectra for monolayer WS_2 grown on hBN (Figure S8), PL spectra of monolayer WS_2 transferred from a SiO_2/Si substrate as a growth substrate onto graphite and another SiO_2/Si substrate (Figure S9), and optical images and Raman spectra of exfoliated graphite and hBN (Figure S10). This material is available free of charge *via* the Internet at http://pubs.acs.org.

Acknowledgment. This work was supported by a Grant-in-Aid for Scientific Research on Innovative Areas (No. 26107530) from the Ministry of Education, Culture, Sports, Science and Technology (MEXT), Japan, and the Izumi Science and Technology Foundation. The authors thank Y. Miyauchi, K. Matsuda (Kyoto University), S. Konabe (Tsukuba University), and K. Nagashio (University of Tokyo) for useful discussions, and K. Kuramoto (Keyence) for conducting the laser microscope observations. Z.L. acknowledges support from the MEXT KAKENHI "Science of Atomic Layers" (Grant No. 25107003). Z.L. and K.S. acknowledge support from a JST Research Acceleration Program.

REFERENCES AND NOTES

1. Wang, Q. H.; Kalantar-Zadeh, K.; Kis, A.; Coleman, J. N.; Strano, M. S. Electronics and Optoelectronics of Two-Dimensional Transition Metal Dichalcogenides. *Nat. Nanotechnol.* **2012**, *7*, 699–712.
2. Chhowalla, M.; Shin, H. S.; Eda, G.; Li, L.-J.; Loh, K. P.; Zhang, H. The Chemistry of Two-Dimensional Layered Transition Metal Dichalcogenide Nanosheets. *Nat. Chem.* **2013**, *5*, 263–275.
3. Radisavljevic, B.; Radenovic, A.; Brivio, J.; Giacometti, V.; Kis, A. Single-Layer MoS_2 Transistors. *Nat. Nanotechnol.* **2011**, *6*, 147–150.
4. Ovchinnikov, D.; Allain, A.; Huang, Y.-S.; Dumcenco, D.; Kis, A. Electrical Transport Properties of Single-Layer WS_2. *ACS Nano* **2014**, *8*, 8174–8181.
5. Zhao, W.; Ghorannevis, Z.; Chu, L.; Toh, M.; Kloc, C.; Tan, P.-H.; Eda, G. Evolution of Electronic Structure in Atomically Thin Sheets of WS_2 and WSe_2. *ACS Nano* **2012**, *7*, 791–797.
6. Mak, K. F.; Lee, C.; Hone, J.; Shan, J.; Heinz, T. F. Atomically Thin MoS_2: A New Direct-Gap Semiconductor. *Phys. Rev. Lett.* **2010**, *105*, 136805.
7. Splendiani, A.; Sun, L.; Zhang, Y.; Li, T.; Kim, J.; Chim, C.-Y.; Galli, G.; Wang, F. Emerging Photoluminescence in Monolayer MoS_2. *Nano Lett.* **2010**, *10*, 1271–1275.
8. Eda, G.; Yamaguchi, H.; Voiry, D.; Fujita, T.; Chen, M.; Chhowalla, M. Photoluminescence from Chemically Exfoliated MoS_2. *Nano Lett.* **2011**, *11*, 5111–5116.
9. Zhang, Y. J.; Oka, T.; Suzuki, R.; Ye, J. T.; Iwasa, Y. Electrically Switchable Chiral Light-Emitting Transistor. *Science* **2014**, *344*, 725–728.
10. Zeng, H.; Dai, J.; Yao, W.; Xiao, D.; Cui, X. Valley Polarization in MoS_2 Monolayers by Optical Pumping. *Nat. Nanotechnol.* **2012**, *7*, 490–493.
11. Mak, K. F.; He, K.; Shan, J.; Heinz, T. F. Control of Valley Polarization in Monolayer MoS_2 by Optical Helicity. *Nat. Nanotechnol.* **2012**, *7*, 494–498.
12. Huang, X.; Zeng, Z.; Zhang, H. Metal Dichalcogenide Nanosheets: Preparation, Properties and Applications. *Chem. Soc. Rev.* **2013**, *42*, 1934–1946.
13. Zhou, W.; Zou, X.; Najmaei, S.; Liu, Z.; Shi, Y.; Kong, J.; Lou, J.; Ajayan, P. M.; Yakobson, B. I.; Idrobo, J.-C. Intrinsic Structural Defects in Monolayer Molybdenum Disulfide. *Nano Lett.* **2013**, *13*, 2615–2622.
14. Mak, K. F.; He, K.; Lee, C.; Lee, G. H.; Hone, J.; Heinz, T. F.; Shan, J. Tightly Bound Trions in Monolayer MoS_2. *Nat. Mater.* **2012**, *12*, 207–211.
15. Mitioglu, A. A.; Plochocka, P.; Jadczak, J. N.; Escoffier, W.; Rikken, G. L. J. A.; Kulyuk, L.; Maude, D. K. Optical Manipulation of the Exciton Charge State in Single-Layer Tungsten Disulfide. *Phys. Rev. B* **2013**, *88*, 245403.
16. Ross, J. S.; Wu, S.; Yu, H.; Ghimire, N. J.; Jones, A. M.; Aivazian, G.; Yan, J.; Mandrus, D. G.; Xiao, D.; Yao, W.; *et al*. Electrical Control of Neutral and Charged Excitons in a Monolayer Semiconductor. *Nat. Commun.* **2013**, *4*, 1474.
17. Jones, A. M.; Yu, H.; Ghimire, N. J.; Wu, S.; Aivazian, G.; Ross, J. S.; Zhao, B.; Yan, J.; Mandrus, D. G.; Xiao, D.; *et al*. Optical Generation of Excitonic Valley Coherence in Monolayer WSe_2. *Nat. Nanotechnol.* **2013**, *8*, 634–638.
18. Tongay, S.; Suh, J.; Ataca, C.; Fan, W.; Luce, A.; Kang, J. S.; Liu, J.; Ko, C.; Raghunathanan, R.; Zhou, J.; *et al*. Defects Activated Photoluminescence in Two-Dimensional Semiconductors: Interplay between Bound, Charged, and Free Excitons. *Sci. Rep.* **2013**, *3*, 2657.
19. Castellanos-Gomez, A.; Roldán, R.; Cappelluti, E.; Buscema, M.; Guinea, F.; van der Zant, H. S. J.; Steele, G. A. Local Strain Engineering in Atomically Thin MoS_2. *Nano Lett.* **2013**, *13*, 5361–5366.
20. Wu, S.; Huang, C.; Aivazian, G.; Ross, J. S.; Cobden, D. H.; Xu, X. Vapor-Solid Growth of High Optical Quality MoS_2 Monolayers with Near-Unity Valley Polarization. *ACS Nano* **2013**, *7*, 2768–2772.
21. van der Zande, A. M.; Huang, P. Y.; Chenet, D. A.; Berkelbach, T. C.; You, Y.; Lee, G.-H.; Heinz, T. F.; Reichman, D. R.; Muller, D. A.; Hone, J. C. Grains and Grain Boundaries in Highly Crystalline Monolayer Molybdenum Disulphide. *Nat. Mater.* **2013**, *12*, 554–561.
22. Lee, Y.-H.; Zhang, X.-Q.; Zhang, W.; Chang, M.-T.; Lin, C.-T.; Chang, K.-D.; Yu, Y.-C.; Wang, J. T.-W.; Chang, C.-S.; Li, L.-J.; *et al*. Synthesis of Large-Area MoS_2 Atomic Layers with Chemical Vapor Deposition. *Adv. Mater.* **2012**, *24*, 2320–2325.
23. Huang, J.-K.; Pu, J.; Hsu, C.-L.; Chiu, M.-H.; Juang, Z.-Y.; Chang, Y.-H.; Chang, W.-H.; Iwasa, Y.; Takenobu, T.; Li, L.-J. Large-Area Synthesis of Highly Crystalline WSe_2 Monolayers and Device Applications. *ACS Nano* **2013**, *8*, 923–930.
24. Orofeo, C. M.; Suzuki, S.; Sekine, Y.; Hibino, H. Scalable Synthesis of Layer-Controlled WS_2 and MoS_2 Sheets by Sulfurization of Thin Metal Films. *Appl. Phys. Lett.* **2014**, *105*, 083112.
25. Okada, M.; Sawazaki, T.; Watanabe, K.; Taniguch, T.; Hibino, H.; Shinohara, H.; Kitaura, R. Direct Chemical Vapor Deposition Growth of WS_2 Atomic Layers on Hexagonal Boron Nitride. *ACS Nano* **2014**, *8*, 8273–8277.
26. Ge, W.; Kawahara, K.; Tsuji, M.; Ago, H. Large-Scale Synthesis of NbS_2 Nanosheets with Controlled Orientation on Graphene by Ambient Pressure CVD. *Nanoscale* **2013**, *5*, 5773–5778.
27. Ling, X.; Lee, Y.-H.; Lin, Y.; Fang, W.; Yu, L.; Dresselhaus, M. S.; Kong, J. Role of the Seeding Promoter in MoS_2 Growth by Chemical Vapor Deposition. *Nano Lett.* **2014**, *14*, 464–472.
28. Shi, Y.; Zhou, W.; Lu, A.-Y.; Fang, W.; Lee, Y.-H.; Hsu, A. L.; Kim, S. M.; Kim, K. K.; Yang, H. Y.; Li, L.-J.; *et al*. van der Waals Epitaxy of MoS_2 Layers Using Graphene as Growth Templates. *Nano Lett.* **2012**, *12*, 2784–2791.
29. Zhang, C.; Johnson, A.; Hsu, C.-L.; Li, L.-J.; Shih, C.-K. Direct Imaging of Band Profile in Single Layer MoS_2 on Graphite: Quasiparticle Energy Gap, Metallic Edge States, and Edge Band Bending. *Nano Lett.* **2014**, *14*, 2443–2447.
30. Gutiérrez, H. R.; Perea-López, N.; Elías, A. L.; Berkdemir, A.; Wang, B.; Lv, R.; López-Urías, F.; Crespi, V. H.; Terrones, H.; Terrones, M. Extraordinary Room-Temperature Photoluminescence in Triangular WS_2 Monolayers. *Nano Lett.* **2012**, *13*, 3447–3454.
31. Miyauchi, Y.; Saito, R.; Sato, K.; Ohno, Y.; Iwasaki, S.; Mizutani, T.; Jiang, J.; Maruyama, S. Dependence of Exciton Transition Energy of Single-Walled Carbon Nanotubes on Surrounding Dielectric Materials. *Chem. Phys. Lett.* **2007**, *442*, 394–399.
32. Wang, Y.; Cong, C.; Qiu, C.; Yu, T. Raman Spectroscopy Study of Lattice Vibration and Crystallographic Orientation of Monolayer MoS_2 under Uniaxial Strain. *Small* **2013**, *9*, 2857–2861.
33. Rice, C.; Young, R. J.; Zan, R.; Bangert, U.; Wolverson, D.; Georgiou, T.; Jalil, R.; Novoselov, K. S. Raman-Scattering Measurements and First-Principles Calculations of Strain-Induced Phonon Shifts in Monolayer MoS_2. *Phys. Rev. B* **2013**, *87*, 081307.
34. Yun, W. S.; Han, S. W.; Hong, S. C.; Kim, I. G.; Lee, J. D. Thickness and Strain Effects on Electronic Structures of Transition Metal Dichalcogenides: 2H-MX_2 Semiconductors (M = Mo, W; X = S, Se, Te). *Phys. Rev. B* **2012**, *85*, 033305.
35. Nelson, J. B.; Riley, D. P. The Thermal Expansion of Graphite from 15 to 800 °C: Part I. Experimental. *Proc. Phys. Soc.* **1945**, *57*, 477–486.
36. Matthäus, A.; Ennaoui, A.; Fiechter, S.; Tiefenbacher, S.; Kiesewetter, T.; Diesner, K.; Sieber, I.; Jaegermann, W.; Tsirlina, T.; Tenne, R. Highly Textured Films of Layered Metal Disulfide 2H-WS_2: Preparation and Optoelectronic Properties. *J. Electrochem. Soc.* **1997**, *144*, 1013–1019.
37. Paszkowicz, W.; Pelka, J. B.; Knapp, M.; Szyszko, T.; Podsiadlo, S. Lattice Parameters and Anisotropic Thermal Expansion of Hexagonal Boron Nitride in the 10 - 297.5 K Temperature Range. *Appl. Phys. A: Mater. Sci. Process.* **2002**, *75*, 431–435.
38. Zhao, J.-H.; Ryan, T.; Ho, P. S.; McKerrow, A. J.; Shih, W.-Y. Measurement of Elastic Modulus, Poisson Ratio, and Coefficient of Thermal Expansion of on-Wafer Submicron Films. *J. Appl. Phys.* **1999**, *85*, 6421–6424.

39. Young, A. F.; Dean, C. R.; Meric, I.; Sorgenfrei, S.; Ren, H.; Watanabe, K.; Taniguchi, T.; Hone, J.; Shepard, K. L.; Kim, P. Electronic Compressibility of Layer-Polarized Bilayer Graphene. *Phys. Rev. B* **2012**, *85*, 235458.
40. Fontanella, J.; Andeen, C.; Schuele, D. Low Frequency Dielectric Constants of Quartz, Sapphire, MgF_2, and MgO. *J. Appl. Phys.* **1974**, *45*, 2852–2854.
41. Cardona, M.; Meyer, T. A.; Thewalt, M. L. W. Temperature Dependence of the Energy Gap of Semiconductors in the Low-Temperature Limit. *Phys. Rev. Lett.* **2004**, *92*, 196403.
42. Taniguchi, T.; Watanabe, K. Synthesis of High-Purity Boron Nitride Single Crystals under High Pressure by Using Ba-BN Solvent. *J. Cryst. Growth* **2007**, *303*, 525–529.